Acta of Bioengineering and Biomechanics
Vol. 4, No. 1, 2002

3D hand modelling and analysis using data-gloves: theory and its application in Parkinson's disease

C. R. ALLEN, Y. SU, D. GENG

Department of Electrical and Electronic Engineering, University of Newcastle upon Tyne,
Email: c.r.allen@ncl.ac.uk, URL: http://www.staff.ncl.ac.uk/c.r.allen/

D. BURN, U. BRECHANY

Regional Neurosciences Centre, Newcastle General Hospital, Westgate Road,
Newcastle upon Tyne, NE1 7RU, United Kingdom

In this application, 3D electromagnetic sensors have been integrated into a data-glove to accurately model and capture the motion of the human hand. By modelling the movement of the human hand, this system has been shown to accurately measure the rest tremor evident in subjects with Parkinson's disease. It was found that 11 sensors were sufficient to model the human hand, including all the phalanges. A capture rate of 10 measurements per 1 s was achieved. A discrete Fourier analysis has been applied to extract the tremor frequency from the sensor data time series. Further an analysis of the instantaneous speed of hand motion has been used to extract clinically significant diagnosis. The technique described is seen to provide an objective and quantitative method for the analysis of clinic conditions such as Parkinson's disease (PD) and essential tremor (ET) as a way to assess the effect of therapeutic interventions.

Key words: 3D imaging systems, posture data glove sensing, Parkinson's disease (PD), tremor, essential tremor (ET), bradykinesia, rest tremor

1. Introduction

Attempts to quantify signs of Parkinsonism date back to the 1920's. Accurate and quantitative assessment of tremor and bradykinesia (slow speed of movement, characteristic of Parkinson's disease) may, however, improve diagnostic specificity and provide un-biased quantification of therapeutic interventions. Methods to assess tremor and bradykinesia may be subdivided into objective quantification techniques and subjective assessments. The latter are commonly used in clinical practice and include patient functional disability scales, patient-completed diaries and subjective physician ratings of severity of signs of disease.

Many objective techniques sample only limited aspects of motor dysfunction. The relationship between pathophysiology, impairment and disability is complex; a problem in one domain does not necessarily predict difficulty in another. Existing physiological tech-

niques to record tremor include accelerometry, electromyography (short- or long-term), computer tracking tasks, graphic digitizing tablets and infrared sensor system [1]. Each of these techniques has their drawbacks and several are time-consuming to perform. Objective tests for bradykinesia are even less satisfactory, and include the Purdue pegboard, and tapping tests between two counters a fixed distance apart. Moreover, the pegboard lacks both specificity and sensitivity. It also suffers from a significant "floor" effect.

In this paper, we apply a novel three-dimensional motion system, developed using a 3D imaging system and the electromagnetic position sensors (hand movement recognition), for use in the recording of upper limb tremors and bradykinesia. The quantitative assessment of frequency in Parkinson's disease was first proposed using a posture dataglove in a number of medical abstract publications by D. J. WARNER et al., but no actual measurement were demonstrated [2], [3].

The 3D medical imaging system [4], [5] used has first been introduced in 1993 to visualize online the position of endoscopes in the human colon, later on, another software system (the "RMR" system) [6] was developed to produce a more realistic endoscope using stored data from the original system.

The objective of this application is to characterize the clinical signs of patients exhibiting clinically probable PD (according to the UK Parkinson's Disease Brain Bank Criteria [7]) and patients with definite essential tremor (according to the TRIG criteria [8]) during the studies.

Ethical approval for this work was obtained from Newcastle and North Tyneside Local Research Ethical Committee.

In this application, the 3D imaging system has been used together with a "dataglove", worn on the dominant hand of the patient. Sensor data provide detailed recording on all the hand phalanges. In Parkinson's disease, the involuntary hand tremor frequency is as fast as 4–5 Hz, decrement Fourier transform is used to analyze this tremor frequency and instantaneous speed is also measured by calculating derivative in raw data-time profile for each experiment.

Fig. 1. The 3D imaging system

The 3D imaging data-glove developed for this medical application is comfortable, light-weighted and do not restrict movement nor affect the motion of the hand during experimentation. Electromagnetic sensors provide a powerful technology for human–computer interaction (HCI) and have been applied to many fields [9]. One particular advantage is that the user may harness the technology easily and routinely by using ready-to-wear articles of clothing, e.g. headsets or data-gloves. Secondly the 3D sensors may simply be plugged into a computer system, allowing the user uninhibited control and interaction with the computer system using the glove arrangement (ref. figure 1).

The sensor measurements have been found to be repeatable and accurate. In this section, the assessment of these parameters of measurement quality are presented. Stability is observed by placing the data-glove at a static position in the magnetic field and analyzing the resulting data captured for both position X, Y, Z and orientation, θ and ϕ, for one of the sensors. Figure 2 shows the variability measured for this static test in terms of a standard deviation from the average value in meter. Repeating this experiment and choosing different sensors, the repeatability is obtained (ref. figure 3). By calculating the relative vibration percentage, the conclusion could be made that the accuracy of the system is higher than other system.

To allow multiple users to access the sensor data simultaneously, a data transmission program has been implemented within this application to transfer the sensor data to different client machine via network, and then the live hand motion can be simulated on line on these client machines.

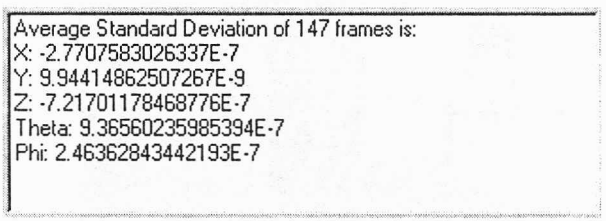

Fig. 2. Stability study

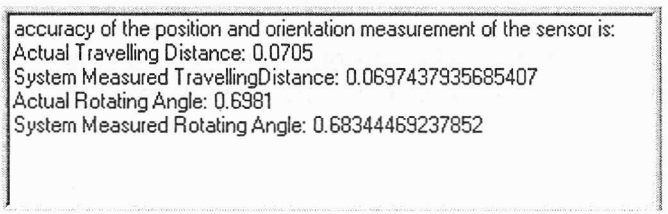

Fig. 3. Repeatability study

Section II describes the principle of the electromagnetic 3D measurement. Section III defines the mathematical model used to construct the on-line graphical hand model. Section IV introduces the algorithm to obtain the frequency of different

movements using the discrete Fourier transform (DFT) and the method to obtain the instantaneous speed of hand movements which is one of the assessments required in the treatment of Parkinson's disease (PD). Section V demonstrates four experiments undertaken to test the capability of the method proposed for (a) the detection of tremor, (b) the rigidity of the wrist during roll motions, (c) the dexterity testing of finger pinching, and (d) hand grip motion using two subjects:

(i) one exhibiting Parkinson's symptoms,

(ii) the other not exhibiting Parkinson's symptoms.

Figure 4 shows a mechanical robot RT100, which is also used in the experiment, the robot is programmed to generate consistent and repeatable motion. It may be therefore used as a reference for the same experiments with human subjects.

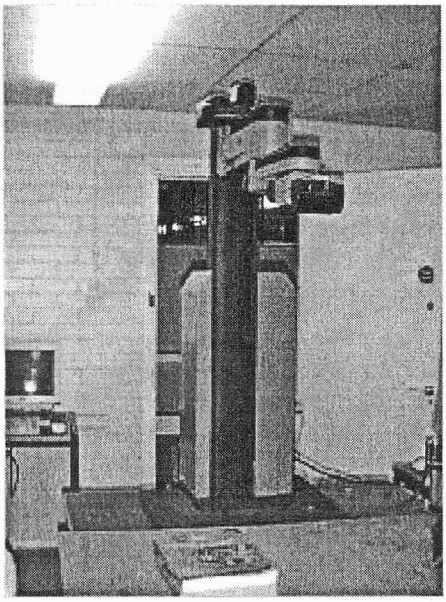

Fig. 4. RT100 robot used to simulate human movement

The results take the form of (1) time-traces for sensors attached to key parts of the hand, (2) a frequency analysis of these time traces, (3) a speed analysis for these time-traces.

2. Principle of 3D electro-magnetic measurement

In order to measure the 3D position and orientation of a sensor, an alternating current (AC) magnetic field must be applied. Each sensor coil then provides an induced voltage that is proportional to the magnetic field strength. For computing the full 3D position and orientation specification of the sensor coil it is necessary to make several

simultaneous measurements. This has required nine generator magnetic sources to be used, which are arranged in three orthogonal sets placed on a horizontal plane. The system is based on low strength magnetic field capable of capturing the absolute position of the magnetic sensor mounted on the data-glove and avoiding the difficulties of calibration of conventional bending sensors. The technique is considered medically safe for use with patients undergoing medical treatment and unlike acoustic and microwave fields, the generators do not need to be in contact with the body or require matching media making the system convenient to use [5].

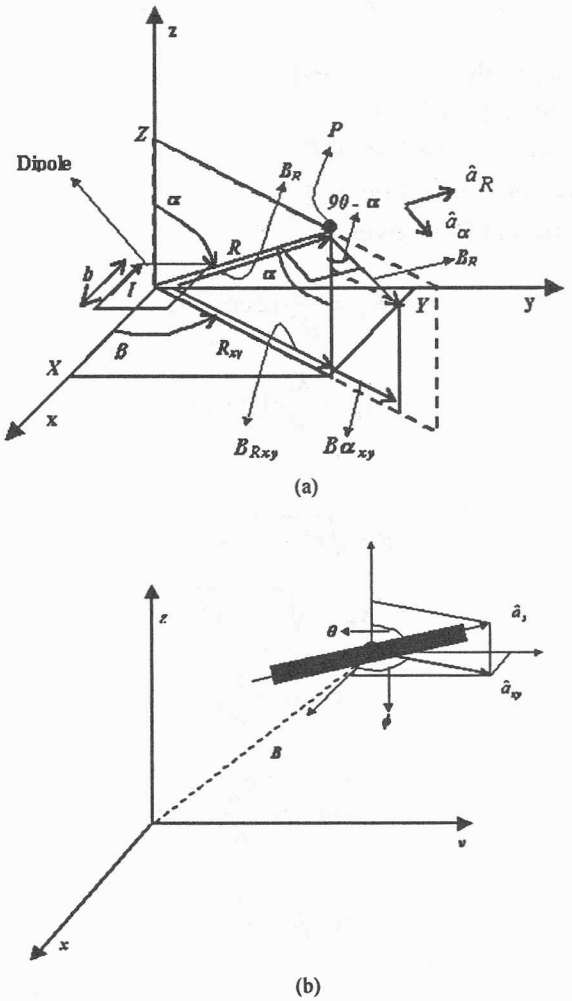

Fig. 5. (a) Diagram for the dipole field equation, (b) 3D sensor in magnetic field

The magnetic field B at a point P, produced by a dipole at the origin (ref. figure 5a), is given by:

$$B = \frac{k_G}{R^3}[2\hat{a}_R \cos\alpha + \hat{a}_\alpha \sin\alpha], \tag{1}$$

where:

B is the magnetic flux density (Tesla),

R is the distance from the dipole to the point P (metres),

α is the angle from the coil axis to the point P (radians),

k_G is a constant equal to $\frac{\mu_0 NIb^2}{4\pi}$, where, $\mu_0 = 4\pi 10^{-7}$, N is the number of turns,

I is the current inside the coil (ampers),

b is the side of the coil (metres),

$\hat{a}_R$ is the unit vector in direction of R,

$\hat{a}_\alpha$ is the unit vector in direction of α.

Deriving the Cartesian form gives:

$$B_R = \frac{k_G}{R^3}(2\cos\alpha), \tag{2}$$

$$B_\alpha = \frac{k_G}{R^3}(\sin\alpha), \tag{3}$$

where:

$$R = \sqrt{x^2 + y^2 + z^2}, \tag{4}$$

$$R_{xy} = \sqrt{x^2 + y^2}, \tag{5}$$

$$\cos\alpha = \frac{z}{R}, \tag{6}$$

$$\sin\alpha = \frac{R_{xy}}{R}, \tag{7}$$

$$\cos\beta = \frac{x}{R_{xy}}, \tag{8}$$

$$\sin\beta = \frac{y}{R_{xy}}. \tag{9}$$

Resolving the fields B_R and B_α produces the following field components:

$$\begin{aligned} B_{xy} &= B_{R_{xy}} + B_{\alpha_{xy}} \\ &= B_R \sin\alpha + B_\alpha \cos\alpha \\ &= \frac{k_G}{R^3}\left[2\cos\alpha\sin\alpha + \sin\alpha\cos\alpha\right] \\ &= \frac{k_G}{R^3}\left[3\cos\alpha\sin\alpha\right] \\ &= \frac{k_G}{R^3}\left[3\frac{zR_{xy}}{R^2}\right], \end{aligned} \tag{10}$$

$$B_x = B_{xy}\cos\beta = \frac{k_G}{R^5}(3xz), \tag{11}$$

$$B_y = B_{xy}\sin\beta = \frac{k_G}{R^5}(3yz), \tag{12}$$

$$\begin{aligned} B_z &= B_R\cos\alpha - B_\alpha\sin\alpha \\ &= \frac{k_G}{R^3}\left[2\cos^2\alpha - \sin^2\alpha\right] \\ &= \frac{k_G}{R^5}\left[2z^2 - y^2 - x^2\right]. \end{aligned} \tag{13}$$

Combining the field components gives:

$$\begin{aligned} B &= B_x\cdot\hat{a}_x + B_y\cdot\hat{a}_y + B_z\cdot\hat{a}_z \\ &= \frac{k_G}{R^5}\left[3z\left(\hat{a}_x x + \hat{a}_y y\right) + \hat{a}_z\left(2z^2 - y^2 - x^2\right)\right]. \end{aligned} \tag{14}$$

Thus for each generator coil with co-ordinates at (X_{Gi}, Y_{Gi}, Z_{Gi} = 0), the magnetic field strength at the measurement sensor is:

$$B_{Gi} = \frac{k_G}{R^5}\left[3z\left(\hat{a}_x(x - X_{Gi}) + \hat{a}_y(y - Y_{Gi})\right) + \hat{a}_z\left(2z^2 - (y - Y_{Gi})^2 - (x - X_{Gi})^2\right)\right], \tag{15}$$

where i is the index reference number for the generator coil. The e.m.f induced in the sensor coil when placed in a magnetic field (ref. figure 5b) is proportional to the resolved component of the field along its axis:

$$V_S = k_S(B\cdot\hat{a}_S), \tag{16}$$

where:

V_S is the e.m.f induced in the sensor (volts),

k_S is a coefficient defining the sensitivity of the sensor (volts/tesla),

$\hat{a}_S$ is the unit vector in direction of the sensor, defined by the two Euler angles θ and ϕ (ref. figure 3).

Expressing the e.m.f induced in the sensor coil related to each generator coil (and their magnetic field), the following equation can be obtained [8]:

$$V_{Si} = \frac{k_G k_S}{R^5}\left\{\left[3z\left(\hat{a}_x x + \hat{a}_y y\right) + \hat{a}_z\left(2z^2 - y^2 - x^2\right)\right]\cdot \hat{a}_S\right\}, \tag{17}$$

where:

$$\hat{a}_S = \left(\sin\theta \cdot \hat{a}_{xy} + \cos\theta \hat{a}_z\right), \tag{18}$$

then $\hat{V}_{Si}$ can be expressed as

$$V_{Si} = \frac{k_G k_S}{R^5}\left\{3z\left[\left(x - X_{Gi}\right)\cos\phi + \left(y - Y_{Gi}\right)\sin\phi\right]\sin\theta + \left[2z^2 - \left(y - Y_{Gi}\right)^2 - \left(x - X_{Gi}\right)^2\right]\cos\theta\right\}. \tag{19}$$

The imaging system consists of three sets generator coils, each set includes three inductive coils, each coil generates a different time varying magnetic field. In total, 9 measurements of the induced voltage of a single sensor are available, therefore, the Cartesian position parameters (x, y, z) and orientation parameters θ and f are obtained. The algorithm used to update the real time sensor position and orientation parameters consists of a seθuence of calculation stages which converts the resolved induced voltage into the final posture measurement. Each stage uses a calibration file to convert the signal into SI units of distance and angle.

Channel	Success	X	Y	Z	Theta	Phi
0		-0.124	0.059	0.292	1.451	-2.326
1		-0.097	0.129	0.301	1.621	-2.072
2		-0.054	0.087	0.311	1.718	-2.311
3		-0.003	0.060	0.277	1.279	-2.886
4	Field out of range	0.061	0.405	0.311	2.474	2.284
5		0.013	0.083	0.310	1.599	-2.464
6		-0.018	-0.015	0.273	1.580	-2.735
7		0.014	0.012	0.291	1.468	-2.822
8		-0.013	-0.072	0.233	1.636	-2.998
9		0.007	0.032	0.327	1.448	-2.768
10		-0.104	0.010	0.302	1.227	-0.932

Fig. 6. On-line position and orientation measurement for the 3D sensors

Stage 1. Convert raw ADC data to volts.
Stage 2. Convert volts to "sensor volts per amp of drive current".
Stage 3. Apply calibration for the generator coils.
Stage 4. Apply calibration for sensor.
Stage 5. Convert result to signed magnitude.
Figure 6 displays a table of position and orientation readings for up to 16 sensors.

3. The mathematical model

In order to measure the position and orientation of the hand in 3D space, it is necessary to attach a set of sensors at strategic positions on a glove. Figure 5 shows the location of

eleven miniature inductive sensors sown into a glove. These sensors are mounted on each fingertip and the phalange above the base joint. One further sensor is put on the palm.

For further operation, we need to label the hand digits from 0 to 4, where 0 is the thumb, and 4 is the little finger. Finger joints are numbered from 0 to 3, where 0 is the base, and 3 is the fingertip (ref. figure 7).

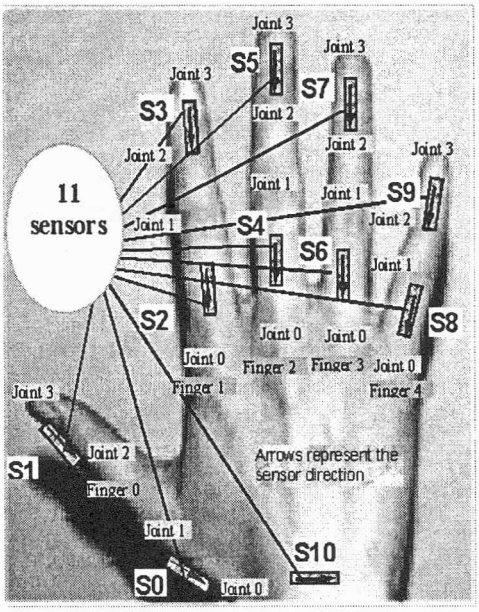

Fig. 7. Sensor positions in the data-glove

3.1. Joint positioning

First, the direction unit vector, converted from the orientation of S10 (ref. figure 7), needs to be scaled by different factors, which is determined by the width of the wrist. Adding or subtracting the position vectors to S10, the position of P1, P2, P3, P4 could be worked out (ref. figures 7, 8).

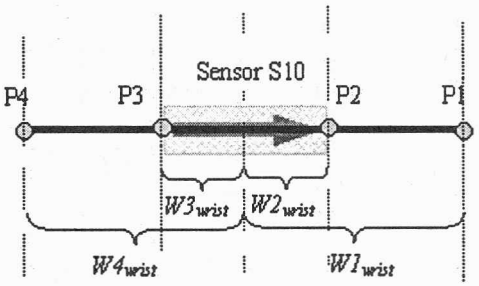

Fig. 8. The definition of wrist vectors

$$\hat{V}_{P1} = \hat{V}_{S10} + \hat{V}_{directionS10} . W1_{wrist}, \tag{20}$$

$$\hat{V}_{P2} = \hat{V}_{S10} + \hat{V}_{directionS10} . W2_{wirst}, \tag{21}$$

$$\hat{V}_{P3} = \hat{V}_{S10} - \hat{V}_{directionS10} . W3_{wrist}, \tag{22}$$

$$\hat{V}_{P4} = \hat{V}_{S10} - \hat{V}_{directionS10} . W4_{wrist}, \tag{23}$$

where:

$\hat{V}_{S10}$ is the position of sensor S10 (ref. figure 7),

$\hat{V}_{directionS10}$ is the unit direction vector of sensor S10,

$W1_{wrist}$, $W2_{wrist}$, $W3_{wrist}$ and $W4_{wrist}$ are the distances from S10 to P1, P2, P3 and P4.

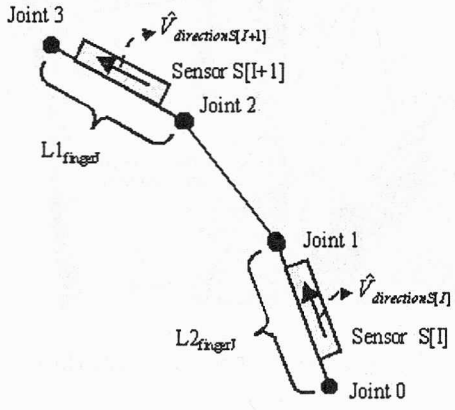

Fig. 9. Measurement of finger positions

The sensors, described above 'on each fingertip' and 'on the phalange above the finger base', are put along and in the middle of that phalange. Then positions of joints 0, 1, 2, 3 of all fingers 0, 1, 2, 3, 4 (ref. figures 7, 9) are determined by scaling the direction unit vector of the relevant sensor with the factor determined by the length of the phalange.

$$\hat{V}_{Joint0} = \hat{V}_{S[I]} - \hat{V}_{directionS[I]} \cdot \left(\frac{L2_J}{2} \right), \tag{24}$$

$$\hat{V}_{Joint1} = V_{S[I]} + \hat{V}_{directionS[I]} \cdot \left(\frac{L2_J}{2} \right), \tag{25}$$

$$\hat{V}_{Joint2} = \hat{V}_{S[I+1]} - \hat{V}_{directionS[I+1]} \cdot \left(\frac{L1_J}{2} \right), \tag{26}$$

$$\hat{V}_{\text{Joint3}} = \hat{V}_{\text{S}[I+1]} + \hat{V}_{\text{directionS}[I+1]} \cdot \left(\frac{L1_J}{2} \right), \tag{27}$$

where:

$\hat{V}_{\text{S}[I]}$ and $\hat{V}_{\text{S}[I+1]}$ are the position of sensors S[I] and S[I + 1],

$\hat{V}_{\text{directionS}[I]}$ and $\hat{V}_{\text{directionS}[I+1]}$ are the unit direction vectors of sensors S[I] and S[I + 1],

$L2_J$ and $L1_J$ are the lengths of the relevant finger phalanges (ref. figure 9).

The joint 0 of fingers 1, 2, 3, 4 and P4, P3, P2, P1 will then be connected to form the basic quadrilateral prisms to draw the palm (figure 7).

3.2. Calculation of the vertices for each face (8)

The shape of a human finger is cylindrical. To render a realistic image, the cylindrical shape is approximated as a series of octagonal prisms following the bending of a human finger. It is very easy to determine a plane in which the joints 1 and 2 should lay by knowing their up-vectors, which could be actually calculated by adding the direction vectors of the two finger bones linked by the proportional joint. Figure 10 shows the octagons constructed around the finger joints. Each of the eight vertices of neighbouring octagons may be joined to form a series of connected quadrilateral prisms around the finger bone.

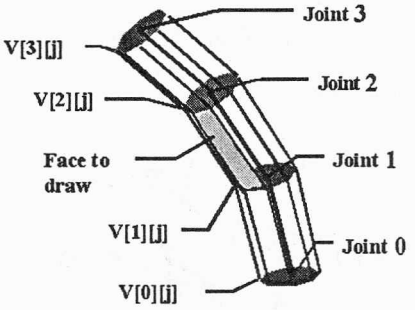

Fig. 10. The octagon shape used to represent the human finger phalanges

3.3. Calculation of facet and surface normals

After creating all the vertices, a series of four-side faces (ref. figure 10) are used to represent the finger surface. For drawing the object in open-GL, the up-vector to each of these faces is calculated (ref. figure 11).

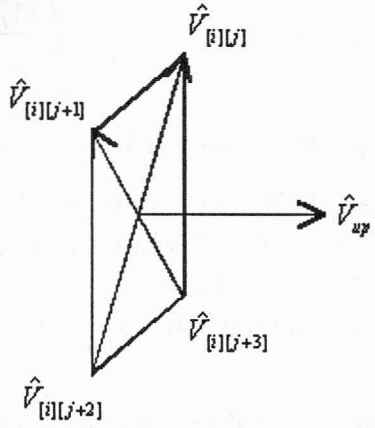

Fig. 11. Up-vector for each polygon face

$$\hat{V}_2 = \hat{V}_{[i][j+2]} - \hat{V}_{[i][j+3]}, \tag{28}$$

$$\hat{V}_1 = \hat{V}_{[i][j]} - \hat{V}_{[i][j+2]}, \tag{29}$$

$$\hat{V}_{up} = \hat{V}_1 \cdot \hat{V}_2, \tag{30}$$

where:

$\hat{V}_{[i][j]}$, $\hat{V}_{[i][j+1]}$, $\hat{V}_{[i][j+2]}$, $\hat{V}_{[i][j+3]}$ are four vertices of a face,

$\hat{V}_{up}$ is the up-vertex of this face.

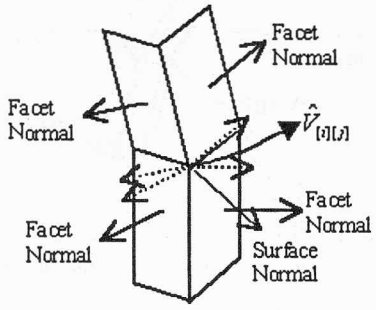

Fig. 12. Surface normals of each of the prism vertices

In order to make the image appear smooth, surface normals should be calculated for each of the prism vertices by adding the facet normals of the four faces by which the vertex is shared and then re-normalized (ref. figure 12) [6].

3.4. Drawing the object

The hand model is written in Delphi Pascal using the open-GL graphics library for 3D-image rendering. It relies on the windowing system for window management, event handling, colour map operations, etc. [10]. The image produced has to be redrawn regularly to give the impression of animation at the display refresh rate of 50 frames per second. Figure 13 shows the images captured from instances of a series real-time hand movement. Whilst the graphic model is displayed, the sensor data to produce each hand frame may be saved to a file for further clinical analysis. Off-line, signal processing algorithms are used to extract motion parameters such as dominant frequency and variation in speed of the hand motion.

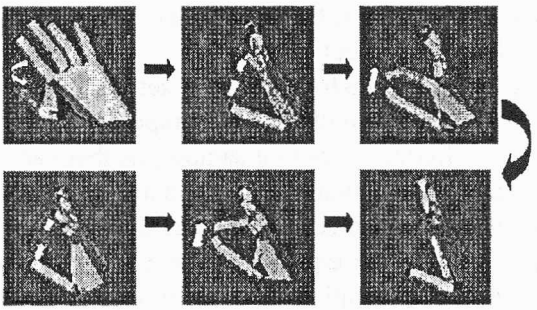

Fig. 13. A sample of the 3D hand model

4. Fast Fourier transform analysis of the recorded data and speed analysis for slowness test

The discrete fast Fourier transform algorithm has been widely used in motion analysis, for example:

- In analysis of digital audio recordings to determine the frequency of a note played in recorded music, to try to recognize different kinds of birds or insects, etc.
- In image motion processing.
- In statistical prediction applications, periodic fluctuations in stock prices, prediction of animal populations.
- In analysis of seismographic data to take "sonograms" of activity inside the Earth.

In this application, the discrete fast Fourier transform algorithm (DFT) has been used to synthesize dominant frequencies in individual sensor data time series. This allows important clinical measures to be defined objectively and with precision. This is seen to offer scientific rigour to what is currently a qualitative assessment of Parkinson's symptoms carried out by medical professionals. The main diagnoses and assessments of Parkinson's disease are bradykinesia, impaired gait and mobility, postural instability, resting tremor and limb rigidity.

The Fourier transform is based on the discovery that it is possible to take any periodic function of time $x(t)$ and resolve it into an equivalent infinite summation of sine waves and cosine waves with frequencies that start at 0 and increase in integer multiples of a base frequency $f_0 = 1/T$, where T is the period of $x(t)$.

$$x(t) = a_0 + \sum_{k=1}^{\infty} [a_k \cos(2\pi k f_0 t) + b_k \sin(2\pi k f_0 t)]. \tag{31}$$

An expression of the form of the right-hand side of this equation is called a Fourier series. The Fourier transform computes the a_k and b_k values to produce the Fourier series, given the base frequency and the function $x(t)$. The a_0 term outside the summation can be considered as the cosine coefficient for $k = 0$. There is no corresponding zero-frequency sine coefficient b_0 because the sine of zero is zero, and therefore such a coefficient would have no effect.

To compute the fast Fourier transform, a finite set of sines and cosines has to be defined. This is easy to do for a digitally sampled input, when we stipulate that there will be the same number of frequency output samples as there are time input samples. In this application, we can pretend that the function $x(t)$ is periodic, and that the period is the same as the length of the recording. The duration of the repeated section defines the base frequency f_0 in the equations above. In other words, f_0 = sampling rate/N, where N is the number of samples in the recording.

The DFT is an algorithm that converts a sampled complex-valued function of time into a sampled complex-valued function of frequency [11]. A rigorous mathematical understanding of the DFT can be expressed in the following equation that tells you the exact relationship between the inputs and outputs:

$$y_p = \sum_{k=0}^{n-1} x_k \left\{ \cos\left[2\pi \frac{kp}{n} \right] + i \sin\left[2\pi \frac{kp}{n} \right] \right\}, \tag{32}$$

where:

x_k is the kth complex-valued input (time-domain) sample,

y_p is the pth complex-valued output (frequency-domain) sample,

$n = 2^N$ is the total number of samples,

k and p are in the range $[0 \ldots n - 1]$.

There are several relationships that must be considered using DFT. The major parameters of interest that will be reviewed here are as follows:

T is increment between time samples (in seconds),

f_s is sampling rate (in hertz) = $1/T$,

F is increment between frequency components (in hertz) = frequency resolution,

t_p is record length (in seconds) = effective period of time signal = $1/F$,

f_0 is folding frequency = $f_s / 2$ (in hertz),

f_h is possible highest frequency in spectrum (in hertz),

N is number of samples in record.

In order to avoid aliasing, it is necessary that

$$f_s \geq 2f_h, \tag{33}$$

this will result in

$$T \leq \frac{1}{2f_h}. \tag{34}$$

For a desired frequency resolution, the minimum record length t_p must be selected according to

$$t_p = \frac{1}{F}. \tag{35}$$

Equations (34) and (35) lead to the conclusion that in order to identify high frequency, it is necessary to reduce T, for a given N, record length t_p would be shorten, thus the frequency resolution will be decreased. Conversely, to increase the resolution, it is necessary to increase t_p, for a given N, T would be increased, which would decrease the ability to identify high frequency.

The only way to satisfy both the ability to identify high frequency and the ability to obtain high-frequency resolution is to increase the number of points N in a record length. If f_h and F are both specified, N must satisfy [12]

$$N \geq \frac{2f_h}{F}. \tag{36}$$

The frequency resolution is not a crucial factor for the study of Parkinson's disease, but to identify the 4–5 Hz tremor frequency the sampling rate has to achieve minimum 10 Hz, which is the highest capacity of the current system.

Applying this technology, a graphic interface has been implemented to describe in a chart the raw data and frequency analysis of various tests on patients with Parkinson's disease.

In corresponding to the practical clinic requirements, a speed analysis program has also been implemented. With the speed–time profile, the slowness in the hand movement of patient with Parkinson's disease can be quantitatively measured. The instant speed is defined as the derivative of the raw data in time profile:

$$S = \frac{df}{dt}, \tag{37}$$

where S represents the instant speed, f is the raw data of the actual movement, and t stands for time.

During experiments, up to 5 Hz bandwidth hand motion for two subjects, a patient with Parkinson's disease and a healthy person, and an anthropomorphic 6-axis Robot manipulator called RT-100 are recorded. Recordings were taken at 10 Hz sample rates for 60 seconds, and then analyzed by the above described algorithm.

5. Experiments and clinic analysis

Quantitative measurement technology has been applied in the four experiments of the assessment for patient with Parkinson's disease; in these experiments, frequency and speed are the subjects to be analyzed.

Experiment 1: rest tremor

During this experiment, the above mentioned two subjects, a patient, a healthy person attempted to maintain body position at rest, for example, hand tremor while resting on lap and robot RT100 programmed to do pitch movement to simulate the hand tremor. These hand tremors were recorded and the position vibration of sensor S5 is calculated and saved into a text file (ref. figure 14) [13], [14].

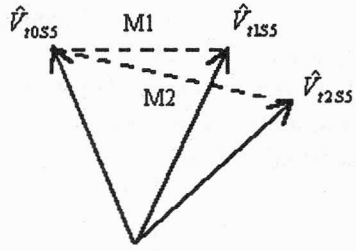

Fig. 14. Rest hand tremor magnitude calculation

$$M1 = \left| \hat{V}_{t0S5} - \hat{V}_{t1S5} \right|, \tag{38}$$

$$M2 = \left| \hat{V}_{t0S5} - \hat{V}_{t2S5} \right|, \tag{39}$$

where:

$M1$, $M2$ are the standard deviations of sensor S5 at different times $t1$ and $t2$ (ref. figure 14),

$\hat{V}_{t0S5}$ is the position of sensor S5 at $t0$,

$\hat{V}_{t1S5}$ is the position of sensor S5 at $t1$,

$\hat{V}_{t2S5}$ is the position of sensor S5 at $t2$.

The results of frequency and speed analysis are displayed in figures 15–18. This test showed that the PD subject had a characteristic tremor frequency at 4.5 Hz (ref. figure 15) which was not apparent in the normal control subject (ref. figure 17). Figures 16, 18 are the speed analysis results of the rest tremor experiment with PD subject and normal control.

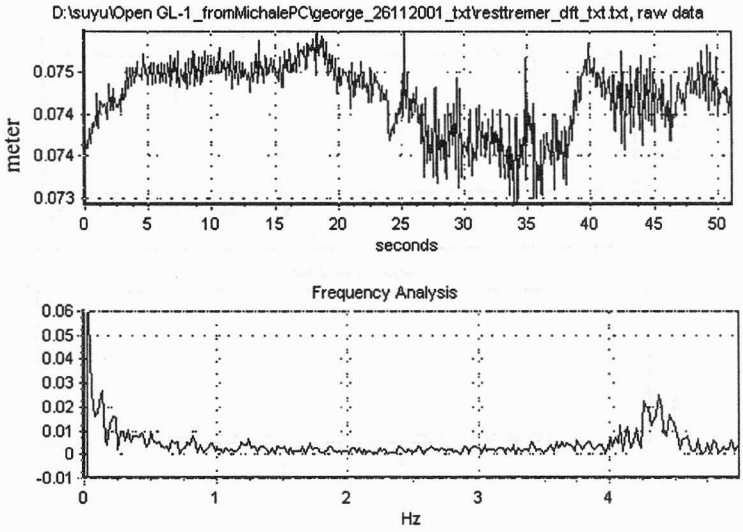

Fig. 15. Rest tremor frequency test result in PD patient

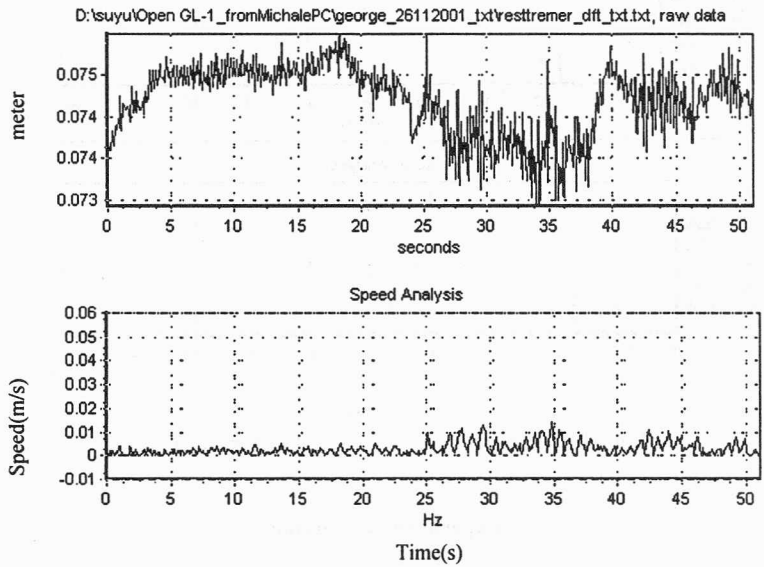

Fig. 16. Rest tremor speed test result in PD patient

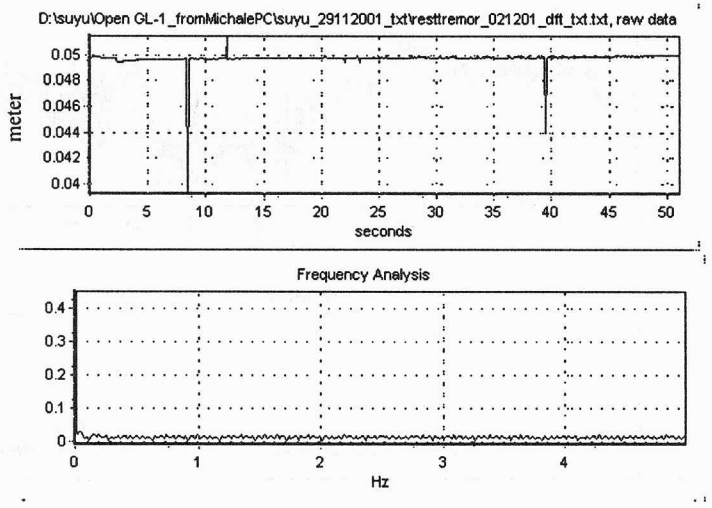

Fig. 17. Rest tremor frequency test result in normal control

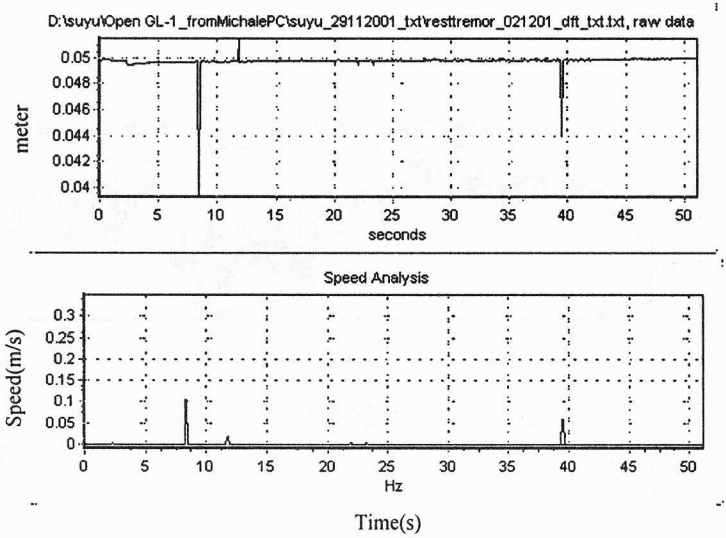

Fig. 18. Rest tremor speed test result in normal control

Experiment 2: Rotation

In this experiment, three subjects, a patient, a healthy person rotated their hands around wrist as much as they can, and robot RT100 programmed to do roll movement with the "wrist" motor to simulate the hand rotation. These hand movements were recorded and rotation angle of sensor S10 (ref. figure 19) was calculated and saved in a text file as the analysis object.

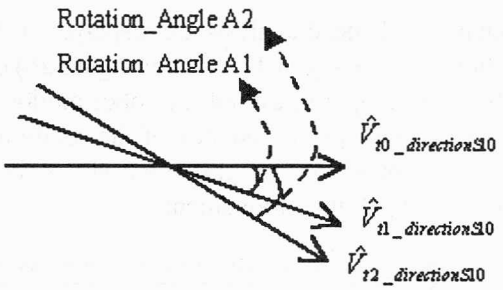

Fig. 19. Hand rotation angle calculation

$$A1 = \cos^{-1}\left(\frac{\hat{V}_{t0\_directionS10} \cdot \hat{V}_{t1\_directionS10}}{\left|\hat{V}_{t0\_directionS10}\right| \cdot \left|\hat{V}_{t1\_directionS10}\right|}\right), \tag{40}$$

$$A2 = \cos^{-1}\left(\frac{\hat{V}_{t0\_directionS10} \cdot \hat{V}_{t2\_directionS10}}{\left|\hat{V}_{t0\_directionS10}\right| \cdot \left|\hat{V}_{t2\_directionS10}\right|}\right), \tag{41}$$

where:

$A1$, $A2$ are the rotation angles from $t0$ to different time $t1$ and $t2$,

$\hat{V}_{t0\_directionS10}$ is the direction vector of sensor S10 at $t0$,

$\hat{V}_{t1\_directionS10}$ is the direction vector of sensor S10 at $t1$,

$\hat{V}_{t2\_directionS10}$ is the direction vector of sensor S10 at $t2$.

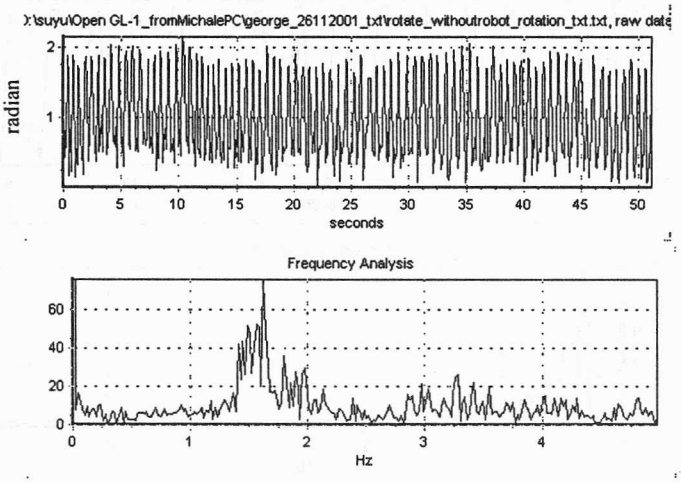

Fig. 20. Rotation frequency test result in PD patient

The results of frequency and speed analysis are displayed in figures 20–25. The PD subject achieved a rotational frequency of 1.5 Hz (ref. figure 20) compared to 0.4 Hz for the normal control subject (ref. figure 22) and the robot motion of 0.8 Hz (ref. figure 24). Figures 21, 23, 25 show the speed tendency of the rotation movement in PD patient, normal control, and robot RT100 programmed with a fixed speed. More speed variation is observed from PD patient's movement.

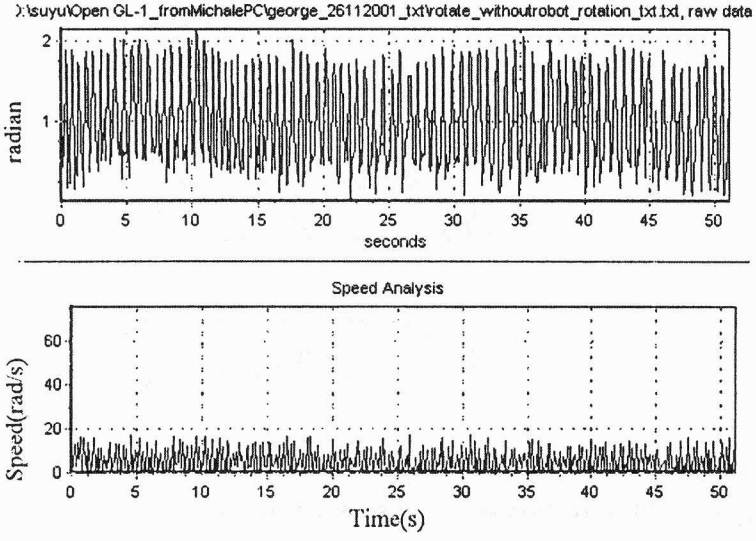

Fig. 21. Rotation speed test result in PD patient

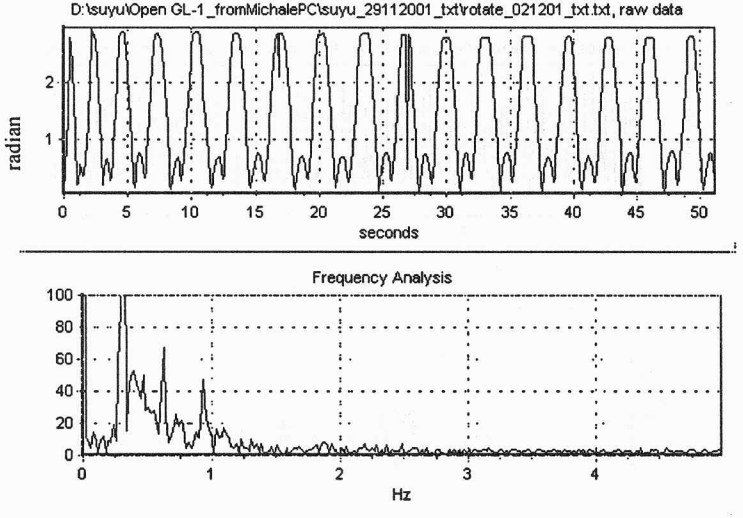

Fig. 22. Rotation frequency test result in normal control

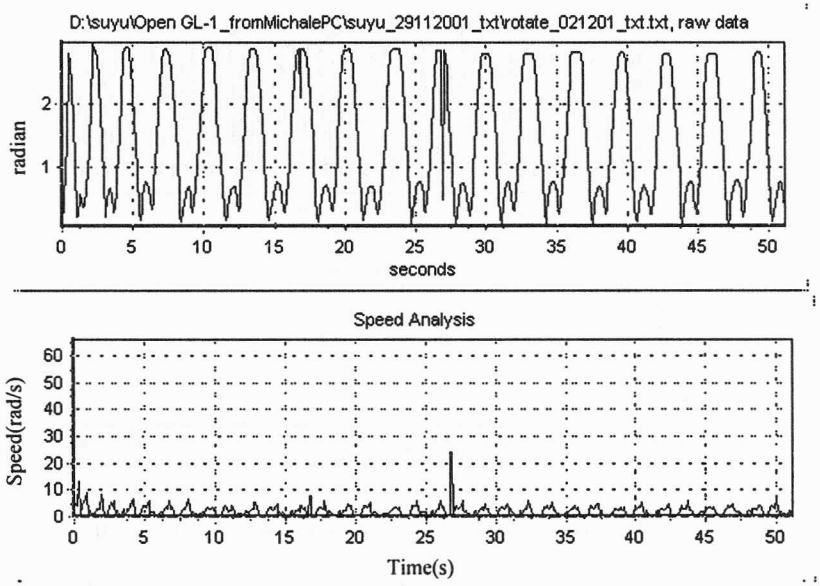

Fig. 23. Rotation speed test result in normal control

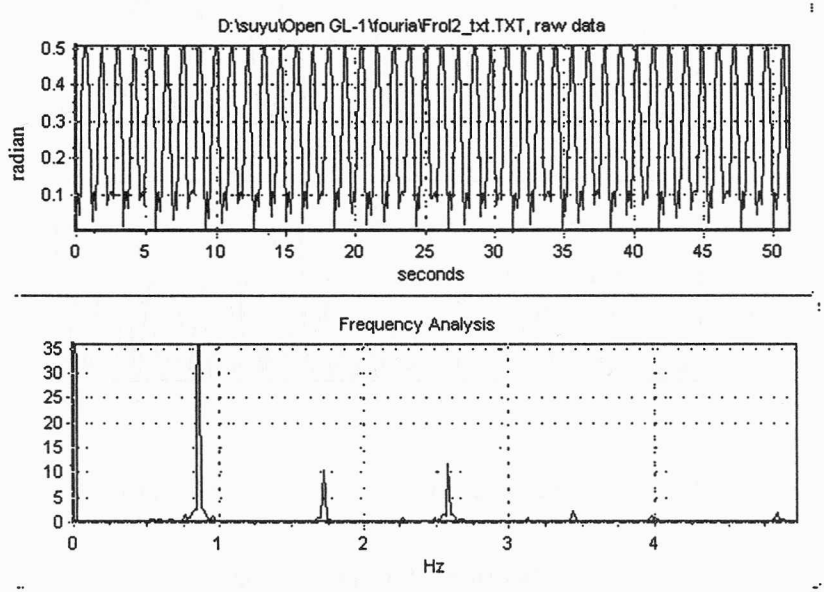

Fig. 24. Fixed speed rotation frequency test result in robot RT100

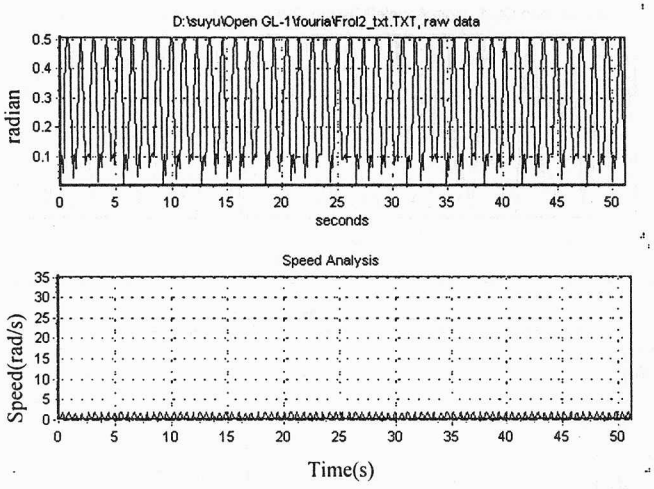

Fig. 25. Fixed speed rotation speed test result in robot RT100

Based on the clinic experience, the rotating speed of a PD patient will be getting lower during the assessment, in order to get the clear observation, robot RT 100 was programmed to roll at a variable speed and the rotating angle is analyzed as shown in figure 26.

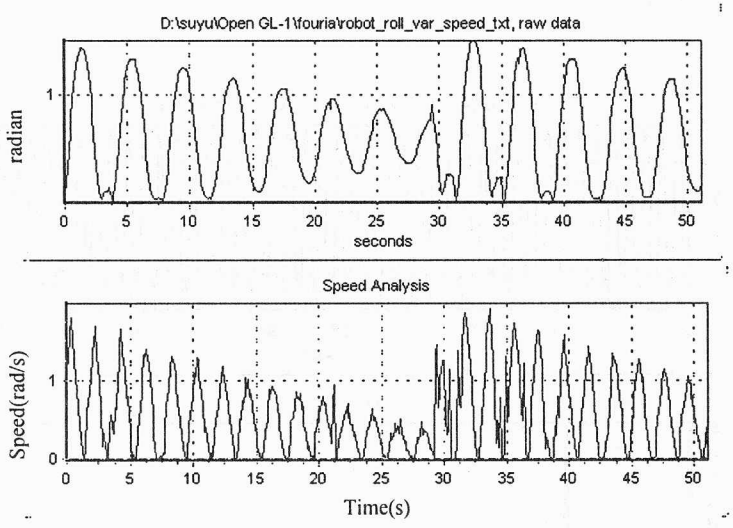

Fig. 26. Variable-speed rotation speed test result in robot RT100

Experiment 3: Finger pinching

In this experiment, a PD patient attempted to grip with his index inger and thumb as much and quickly as possible. This grip movement was recorded and the instanta-

neous distance between sensor S1 and sensor S3 is calculated (ref. figure 27) and saved as the analysis object.

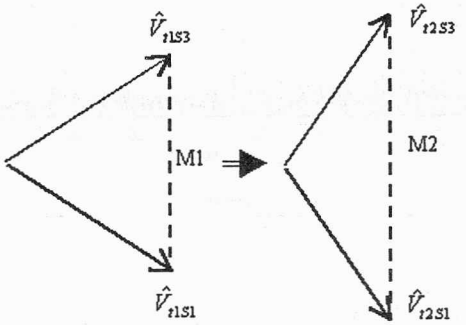

Fig. 27. Calculation of finger pinching motion

$$M1 = \left| \hat{V}_{t1S3} - \hat{V}_{t1S1} \right|, \tag{42}$$

$$M2 = \left| \hat{V}_{t2S3} - \hat{V}_{t2S1} \right|, \tag{43}$$

where:

$M1$, $M2$ are the distances between sensors S3 and S1 at different time $t1$ and $t2$ (ref. figure 27),

$\hat{V}_{t1S3}$ and $\hat{V}_{t1S1}$ are the positions of sensors S3 and S1 at $t1$; $\hat{V}_{t2S3}$ and $\hat{V}_{t2S1}$ are the positions of sensors S3 and S1 at $t2$.

The frequency and speed analysis results are displayed in figures 28, 29. Figure 28 shows that the frequency of this movement in PD subject is 2.8 Hz. Speed variation in this movement can be observed from figure 29.

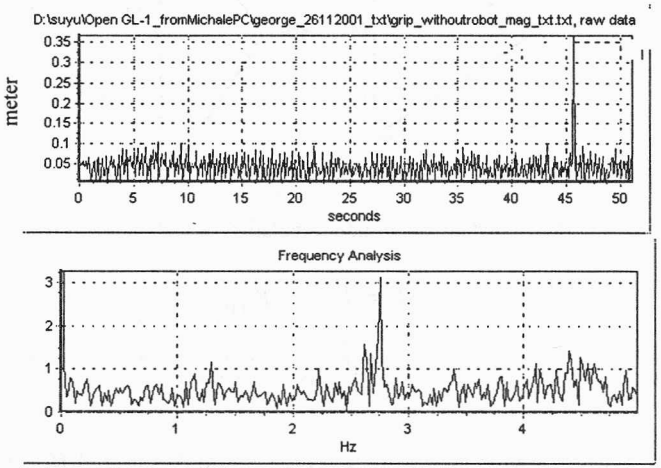

Fig. 28. Finger pinching frequency measurement for the PD patient

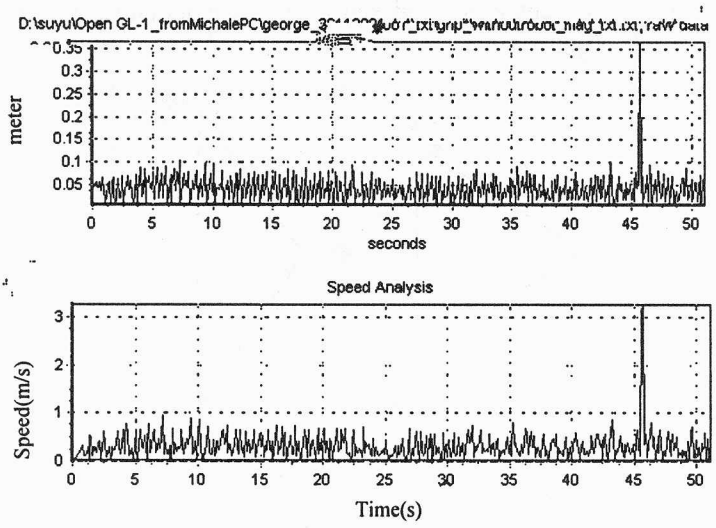

Fig. 29. Finger pinching speed measurement for the PD patient

Experiment 4: grabbing test

This experiment is similar to the grip experiment, the PD patient and a healthy person attempted to grab their hands as much and quickly as possible. Instead of calculating the distance between sensors S1 and S3 (ref. figure 27), the distance between sensors S1 and S5 is measured for further analysis (ref. figure 30).

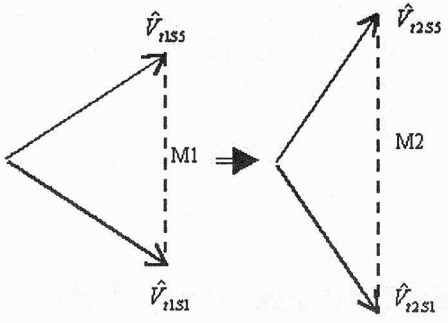

Fig. 30. Instant magnitude calculation of grab movement

$$M1 = \left| \hat{V}_{t1S5} - \hat{V}_{t1S1} \right|, \tag{44}$$

$$M2 = \left| \hat{V}_{t2S5} - \hat{V}_{t2S1} \right|, \tag{45}$$

where:

$M1$, $M2$ are the distances between sensors S5 and S1 at different time $t1$ and $t2$ (ref. figure 30),

$\hat{V}_{t1S5}$ and $\hat{V}_{t1S1}$ are the positions of sensors S5 and S1 at $t1$,

$\hat{V}_{t2S5}$ and $\hat{V}_{t2S1}$ are the positions of sensors S5 and S1 at $t2$.

The frequency and speed analysis results are displayed in figures 31–34. The DFT traces show that the grabbing motion for the PD patient has two dominant frequencies at 2 and 4 Hz (ref. figure 31), whilst the normal control subject has a more distinct motion frequency at 1Hz (ref. figure 33). Large speed variation of the PD patient's grabbing motion can be observed from figure 32 compared to relatively small speed variation (ref. figure 34) of the normal control's grabbing motion.

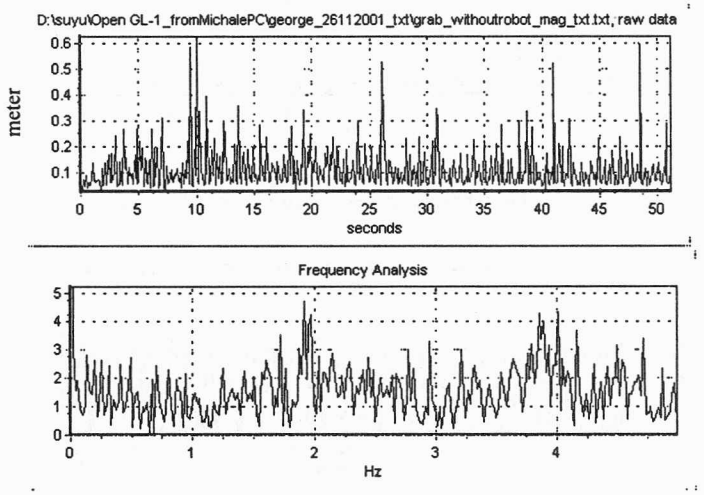

Fig. 31. Grab frequency test result in PD patient

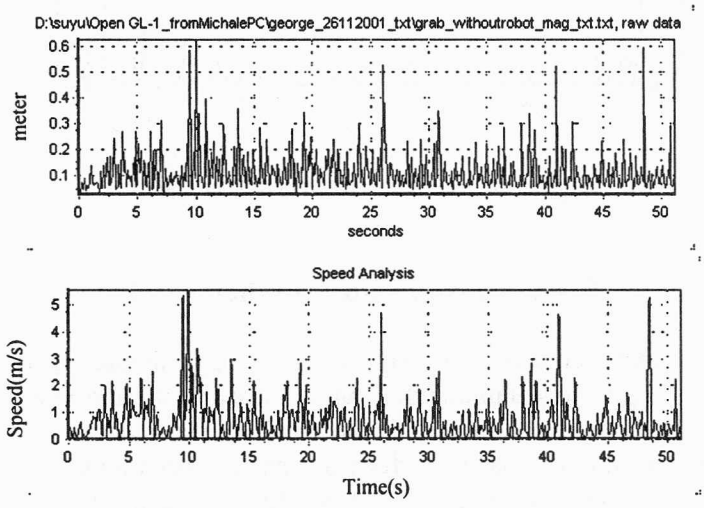

Fig. 32. Grab speed test result in PD patient

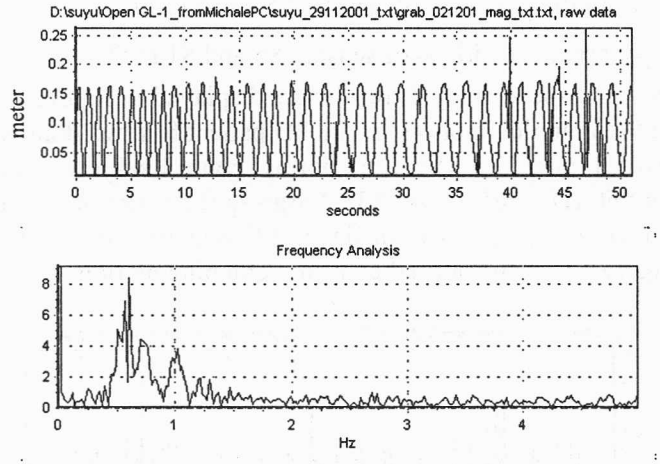

Fig. 33. Grab frequency test result in normal control

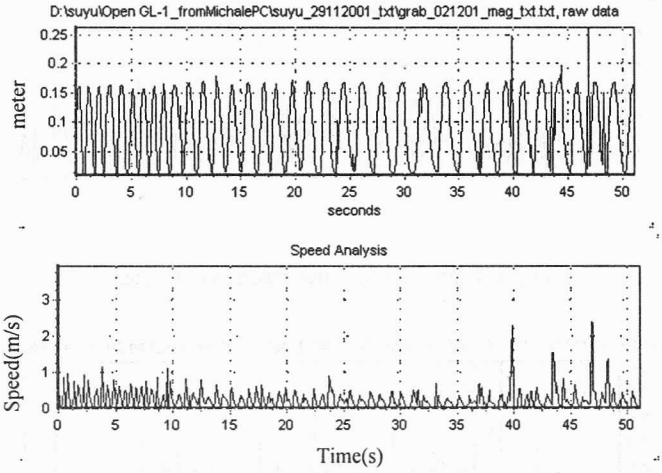

Fig. 34. Grab speed test result in normal control

6. Conclusions and further work

In repeated experiments with the subjects and robot simulator, the system was found to offer a highly repeatable and accurate measure of hand motion of 5 Hz in over the 0.4 m operating range achievable with the system.

The graphical hand model has been described and has been found to play an important role in clinical assessment. Firstly it shows clearly whether the system is operating correctly, checking visually the status of each sensor and whether the hand is within range of measurement. Secondly it shows particular motion characteristics well for

clinical professionals, for example the extent and frequency of essential tremors and the speed changes that occur during wrist rotation or finger pinching measurement.

By using off-line analysis the graphical recording of the hand motion may be used to clinically relevant parameters of movement in patients with two common disorders, essential tremor and Parkinson's disease can be realistically recorded and simulated for both clinical practice and research purpose. Two examples have been provided in sections III and V using the DFT frequency analysis algorithm to extract the essential tremor measurement and the instantaneous sensor speed measurement.

The application of a data-glove with a 3D electromagnetic imaging system objectively records data for the three cardinal features of Parkinson's disease: tremor, rigidity and bradykinesia. Figure 13 has shown that the frequency of essential tremor may be recorded using this technique and was found to be 4.5 Hz. Measurement of the essential tremor present in subjects is currently not possible with the 3D imaging system used in this study. The measurement speed would have to be at least doubled to 20–30 frames/s in order to capture the frequency of essential tremor. This goal will be further researched in the near future with a redesigned higher performance image capture system.

The method is considered to have potential benefit in a number of areas:

- more accurate diagnosis,
- recording progression of disease,
- monitoring the effects of therapeutic interventions.

The motor features of Parkinson's disease are notoriously variable, particularly in the moderate to advanced stages of the illness and any user-friendly system to provide greater objectivity would be greatly welcome by clinicians.

In addition, a quantitative force measurement system is also used in this study to provide an objective assessment of rigidity in Parkinson's disease. A pair of Datacq® gloves incorporating a set of force transducers is utilized together with a force triggering facility controlled by a PC [15]. During the assessment of tone, while the doctor, who wears the gloves, flexes and extends patient's wrist, the force applied is fed back to the force triggering system, recorded and saved on hard-drive for further medical analysis. Meanwhile, force data is drawn into a chart marrying the existing 3D-motion system.

References

[1] BAIN P., *Clinical measurement of tremor*, Mov Disord., 1998, 13, 77–80.

[2] WARNER D.J., WILL A.D., PETERSON G.W., PRICE S.H., SALE E.J., LOMA LINDA C.A., *The VPL Data Glove as a Tool for Hand Rehabilitation and Communication*, Annals of Neurology, 1990, 28, 272.

[3] WILL A.D., WARNER D.J., PETERSON G.W., PRICE S.H., SALE E.J., LOMA LINDA C. A., *Quantitative Analysis of Tremor and Chorea Using the VPL Data Glove*, Annals of Neurology, 1990, 28, 299.

[4] BLADEN J.S., ANDERSON A.P., BELL G.D., RAMEH B., EVANS B., HEATLEY D.J.T., *Non-radiological imaging of endoscopes*, Lancet, 1993, 341, 719–722.

[5] BLADEN J.S., *Electromagnetic imaging system for colonoscopy*, Ph.D. thesis, Sheffield University, 1995.

[6] ROWLAND R.S., BELL G.D., *Non-radiological technique for 3D imaging of intestinal endoscopes: computerised graphical 3D representation of endoscope and skeleton,* Med. Biol. Eng. Comput., 1998, 36, 285–290.

[7] GIBB W.R.G., LEES A.J., *The relevance of the Lewy body to the pathogenesis of idiopathic Parkinson's disease*, Journal of Neurology, Neurosurgery and Psychiatry, 1988, 51, 745–752.

[8] DEUSCHL G., ZIMMERMAN R., GENGER H., LUCKING C.H., *Physiologic classification of essential tremor*, [In:] Findley L.J. and Koller W.C. (eds.), *Handbook of tremor disorders*, New York, NY, Marcel Dekker, 1995, 195–208.

[9] PIMENTAL K., TEIXEIRA K., *Virtual reality through the new looking glass*, Windcrest McGraw Hill, 1992.

[10] AMMERAAL L., *Programming Principles in Computer Graphics*, 2nd edition, Wiley Professional Computing, 1992.

[11] SMITH S.W., *The Scientist and Engineer's Guide to Digital Signal Processing*, California Technical Publishing, 1997.

[12] STANLEY W.D., *Digital Signal Processing*, Reston Publishers, 1975.

[13] YOUNG R., *Update on Parkinson's disease*, Am. Fam. Physician., 1999, Apr. 15, 59(8), 2155–2167, 2169–2170.

[14] SCHIM, *CMEA Medicine Lecture*, 2001, San Diego //for rigidity if involved.

[15] ALLEN C.R., KARAM Z.K., LeCAM P., *In-situ quantification of manual assembly forces and postures during the manufacture of TV deflection coils*, Mechatronics, 1997, 7, 141–157.